Urban Climate 24 (2018) 299–310

Contents lists available at ScienceDirect

Urban Climate

journal homepage: http://www.elsevier.com/locate/uclim

Remote sensing retrieval of urban land surface temperature in hot-humid region

Yurong Shi, Yufeng Zhang *

State Key Laboratory of Subtropical Building Science, Department of Architecture, South China University of Technology, NO 381.Wushan road, Tianhe district, 510640 Guangzhou, PR China

ARTICLE INFO

Article history:
Received 19 October 2016
Received in revised form 3 January 2017
Accepted 4 January 2017

Keywords:
Land surface temperature
Urban climate
Remote sensing
Mono-window algorithm
Field observation

ABSTRACT

With the rapid urbanization and the global climate change, the urban climate problems become increasingly serious in the hot-humid region of China. This study established the satellite-based remote sensing retrieval methods for urban land surface temperature (LST) based on the mono-window algorithm and the estimation methods of ground emissivity and atmospheric transmittance. Through retrieving LST of Haizhu district in Guangzhou in a sunny summer day, it was found that the retrieval methods were able to distinguish the surface temperature variations for different underlying urban surfaces. By comparison with the field observations, it was found that the error of the retrieval methods was about 1.0 °C and the methods were applicable for LST retrieval in the cities in the hot-humid region. By applying the retrieval methods, it showed that the cooling effects of water and vegetation on surrounding urban lands were effective within distances of 250 m and 350 m, respectively. The water cooling effect correlated with its area and width positively, and the vegetation LST correlated with its canopy density negatively. The present study provides reliable techniques for observing and evaluating urban LST and useful guidance for planning and design of urban climate in the hot-humid region.

© 2017 Elsevier B.V. All rights reserved.

1. Introduction

With the rapid urbanization and the global climate change, the urban environment and climate problems become increasingly serious in China. In the hot-humid region of China, the summer is long, hot and humid, and the urban climate problem is severe. On one hand, mortality increases with urban warming. For instance,

* Corresponding author.
E-mail addresses: arshiyurong@mail.scut.edu.cn (Y. Shi), zhangyuf@scut.edu.cn (Y. Zhang)

http://dx.doi.org/10.1016/j.uclim.2017.01.001
2212-0955 © 2017 Elsevier B.V. All rights reserved.

the mean daily count of non-accidental death reached 32.6 during 2006 to 2009 and the temperature-mortality relationship showed a U shape in Guangzhou, a big city in the hot-humid region of China (Wu et al., 2013). On the other hand, building energy consumptions increase with urban warming. For example, a 10% increase in air-conditioning demand was caused by the heat island in Hong Kong (Chan, 2011). The neighborhood microclimate, as the micro-scale of urban climate, relates to people's daily life very closely (Roth et al., 1989). It is thus important and necessary to study the urban climate and the neighborhood microclimate in the hot-humid region for improving living environmental quality, reducing building energy consumption and mitigating urban heat island.

Previous studies on urban climate and neighborhood microclimate are mainly focused on filed study of individual cases and hard to be generalized. On the other side, the advanced technologies of remote sensing are mainly applied to large-scale fields like agriculture and ocean. Only a few studies have been carried out in the cities of Singapore (Nichol, 1996), Tel-Aviv (Saaroni et al., 2000), Salt Lake Valley (Gluch et al., 2006) and China (He and Xu, 2012; Ye, 2009; Wang and Zhang, 2010). The primary work of utilizing remote sensing to urban climate and neighborhood microclimate studies is to acquire land characteristic parameters retrieved by remote sensing techniques. Land surface temperature (LST) has been proved to be an important factor controlling the physical, chemical and biological processes on Earth's surface (Qin and Karnieli, 1999). In the recent years, the remote sensing techniques that based on satellite and aircraft have been advanced greatly and applied extensively in urban climate, for instance, Voogt and Oke (1997, 1998) and Chen et al. (2014) have done many works on urban climate by remote sensing techniques. By using the remote sensing techniques, it can acquire the urban climatic information quickly and broadly and provide a large number of neighborhood microclimatic data by taking its advantages on macro, multiband and high resolution.

This paper aimed at establishing remote sensing retrieval methods for urban LST based on previous studies and testing performances of the retrieval methods through field observations in the city in the hot-humid region of China. Furthermore, the cooling effects of water and vegetation on urban LST will be quantitatively studied by using the validated methods. This study provides reliable methods for remote sensing retrieval of urban LST, and useful guidance for urban climate planning and design in the hot-humid region.

2. Retrieval methods

2.1. Mono-window algorithm

There are three methods, i.e., atmospheric correction method (also called radiative transfer equation), mono-window algorithm (Qin et al., 2001), and single channel algorithm (Jimenez-Munoz and Sobrino, 2003), appropriate for retrieving LST by using the satellite thermal band data. The atmospheric correction method needs to know the in situ atmospheric profile data. It is complicated and hard to acquire and huge error would be produced by its estimation. The mono-window algorithm and the single channel algorithm are both derived from the thermal radiance transfer equation, which are simple, needing few inputs and with relatively less error. Some studies compared the three methods with the field observations in the Chinese cities of Beijing (Bai et al., 2008) and Gansu (Meng et al., 2005), and concluded that the accuracy of the mono-window algorithm was highest for retrieving LST. Therefore, the mono-window algorithm was determined to be the method for retrieving urban LST in the present study.

The mono-window algorithm retrieves LST (T_s) by knowing ground emissivity, effective mean atmospheric temperature and atmospheric transmittance by Eqs. (1)–(3):

$$T_s = [a(1-C-D) + [b(1-C-D) + C + D]\, T_6 - DT_0]/C \tag{1}$$

$$C = \varepsilon\tau \tag{2}$$

$$D = (1-\tau)[1 + (1-\varepsilon)\tau] \tag{3}$$

where a and b are constants, $a = -67.355351$, and $b = 0.458606$; T_6 is the brightness temperature in K; T_0 is the effective mean atmospheric temperature in K; ε is ground emissivity; τ is atmospheric transmittance.

T_6 can be calculated by using the formulas provided for various satellites. T_0 can be evaluated by analysis of the standard atmosphere profile data and the variations of atmospheric moisture and air temperature with the increasing elevation. The methods for estimations of ε and τ are presented in the following sections.

2.2. Ground emissivity estimation

For the remote sensing images, land surfaces can be divided into water, soil, vegetation and mixed pixels. The mixed pixels are most common in the sensing remote images of urban surfaces. The NDVI threshold method proposed by Valor and Caselles (1996) is the most widely used method to estimate ground emissivity of the mixed pixels. It estimates ground emissivity by using the values of NDVI and green coverage ratio.

The present study adopted the improved model proposed by Li et al. (2004) to obtain green coverage ratio (P_v) of the mixed pixels:

$$P_v = \left[(NDVI - NDVI_{Soil}) / \left(NDVI_{Veg} - NDVI_{Soil}\right)\right] \tag{4}$$

where NDVI is normalized differential vegetation index; $NDVI_{Soil}$ and $NDVI_{Veg}$ are normalized differential vegetation index of soil and vegetation, set as empirical values of 0.05 and 0.7, respectively.

The NDVI threshold method was promoted by Qin et al. (2004), which was adopted to estimate ground emissivity of the urban land surface.

$$\varepsilon = P_v R_v \varepsilon_v + (1 - P_v) R_m \varepsilon_m + d\varepsilon \tag{5}$$

where ε is ground emissivity; ε_v and ε_m are emissivity of vegetation and building surface, respectively, set as empirical values of 0.986 and 0.970; $d\varepsilon$ is interaction of thermal radiation between vegetation and building surface, ignored when the land surface is relatively even; R_v and R_m are temperature ratio of vegetation and building surfaces, calculated by the empirical equations:

$$R_v = 0.9332 + 0.0585 P_v \tag{6}$$

$$R_m = 0.9886 + 0.1287 P_v \tag{7}$$

Combining Eqs. (5)–(7), ground emissivity of the mixed pixels in the urban remote sensing images can be estimated by:

$$\varepsilon = 0.9589 + 0.086 P_v - 0.0671 P_v^{\,2} \tag{8}$$

2.3. Atmospheric transmittance estimation

Atmospheric transmittance is affected by various factors like air pressure, air temperature, water vapor content, aerosol content, and concentrations of CO_2, O_3, CO, NH_4 etc. The atmospheric simulation programs such as 6S, LOWTRAN and MODTRAN can be used to estimate atmospheric transmittance. In addition, many studies found that water vapor content is a key factor affecting atmospheric transmittance, and the higher the water vapor content, the lower the atmospheric transmittance is. Mao and Qin (2004) mentioned that it would improve the real-time performance of atmospheric transmittance estimation by using the relationship between water vapor content and thermal infrared band transmittance.

The water vapor content was estimated using Kaufman and Gao's (1992) model in the present study as follows:

$$\omega = \left(\frac{\alpha - \ln\left(\frac{\rho 19}{\rho 2}\right)}{\beta}\right)^2 \tag{9}$$

where ω is water vapor content in g/cm^2; α and β are coefficient, set as 0.02 and 0.651, respectively; $\rho 2$ and $\rho 19$ are the wavelength of band 2 (0.841–0.876 μm) and band 19 (0.915–0.965 μm) for MODIS satellite.

3. Research methods

3.1. Climate and site

Guangzhou, located at latitude 23°08′N and longitude 113°19′E, is a typical example of a city in the hot-humid region of China. The long summers are hot and humid with plentiful rainfall and the winters are warm and short. The monthly mean temperature is 28.4 °C and the humidity is 83% in July and 13.3 °C and 74%, respectively, in January. The prevalent wind is southeast wind in summer and north wind in winter and the annual sunshine hours is 1906 h. The present study was conducted in Guangzhou.

The site to be studied is located in the west part of Haizhu district in Guangzhou as shown in Fig. 1. The site is a typical residential area and consists of many neighborhoods. Most buildings are high-rise and in compact arrangement, and few are low-rise. The greening is continuously distributed. There are verdant trees in the neighborhoods and sparse trees along both sides of the roads. The exterior surfaces of buildings are mainly light tiling and few are plaster. The roadways are covered by asphalt.

3.2. Data acquisition and process

Currently, the satellites of MODIS, ASTER, Landsat have thermal band data, of which, the data of Landsat is easy to acquire and in high resolution. The Landsat has three thermal band sensors, TM, ETM +, and TIRS, and their spatial resolutions are 120 m, 60 m, 100 m, respectively. The Landsat thermal band data was used in the present study. By checking the data passed through Guangzhou in recent time, it was found that the data at GTM 2:51 am (local Time 10:51 am), September 18, 2016, was appropriate for LST analysis because it was sunny and cloudless at that time.

The LST of the whole Haizhu district in Guangzhou was retrieved by using the methods in Section 2, and the detailed data acquisition and process are illustrated as follows.

3.2.1. Spectral radiance

The spectral radiance (L_6) of thermal band 10 from TIRS sensor was acquired by using the function of radiometric calibration of the software ENVI.

Fig. 1. Visible image map of the studied site.
(From Quick birth, 2010).

3.2.2. Brightness temperature

The brightness temperature (T_6) that corresponds to the spectral radiance (L_6) was calculated by using the approximate form of Planck's radiance function:

$$T_6 = K_2 / \ln(1 + K_1/L_6) \quad (10)$$

where K_1 and K_2 were acquired from the header file of the Landsat satellite data, for the TIRS data, $K_1 = 774.89$ W/(m^2·μm·sr), $K_2 = 1321.08$ K.

3.2.3. Effective mean atmospheric temperature

Qin et al. (2003) provided four linear relationships between T_0 and T_a for various standard atmosphere conditions. The relationship for the tropical standard atmosphere condition was used in the present study according to Deng (2010), that is:

$$T_0 = 17.9769 + 0.91715T_a \quad (11)$$

where T_a is near surface air temperature and can be replaced by the local meteorological observation data of daily mean air temperature at the day of satellite passing.

3.2.4. Atmospheric transmittance

The water vapor content was calculated by Eq. (9). Qin et al. (2003) and Gu et al. (2011) studied the changes of atmospheric transmittance with water vapor content (0.4–6.4 g/cm^2) for the mid-latitude atmosphere conditions by using LOWTRAN7 and MODTRAN4, and found that the good linear relationships existed between atmospheric transmittance and water vapor content. This study utilized MODTRAN4 to calculate the atmospheric transmittance in the thermal band of 10.40– 12.50 μm by using the atmospheric profile data of subtropical 30° N in July.

3.2.5. Ground emissivity

The ground emissivity of the site was estimated by the methods in Section 2.2, i.e., the NDVI value was calculated by software ENVI, the green coverage ratio was obtained by Eq. (4), and the ground emissivity was estimated by Eq. (8).

3.3. Field observations

Since field observation of LST for the whole site was not feasible, a small and representative patch of the site was selected as shown in Fig. 2a. The land surface of the patch consists of buildings, vegetation, and

Fig. 2. The observed patch and the measurement method. a The observed patch. b The thermal infrared camera.

roads. The buildings are middle-rise and high-rise. The green coverage ratio ranges from 4% to 28% and the roads cover 20% of the surface. All of these characteristics are close to those of the whole site, indicating that the selected patch is representative to the site in the aspect of land surface.

Thermal Infrared images of the patch were photographed at the time when the Landsat satellite passed through. The instrument is NEC Avio TH9260 Thermal Infrared camera, and its measuring range is −40 to 500 °C, precision is ±2 °C and resolution is 0.06 to 0.12 °C. The camera was fixed at the roof of a tall building near to the patch (Fig. 2b), 84 m above the ground, taking photos from top to bottom. The view angle was approximated to be 30°. The LST of the patch was obtained after emissivity correction, of which the emissivity was set to be 0.97 according to the retrieval results.

4. Results

4.1. The retrieval parameters

The mean near-surface air temperature (T_a) was 28.7 °C for the site at the time the Landsat satellite passed through, based on which, the effective mean atmospheric temperature (T_0) was obtained as 294.8 K. The water vapor content was 4.5 g/cm^2, which is in agreement with the previous findings in the hot-humid region. The atmospheric transmittance was 0.39, the NDVI values changed from −0.03 to 0.43, and the ground emissivity was in range of 0.955– 0.986.

Fig. 3 shows the results of green coverage ratio for the site. It is shown that in the majority of the site the green coverage ratio was between 4% and 28%.

4.2. LST retrievals

The retrieved LST image map of the whole Haizhu district is shown in Fig. 4, of which, the scopes marked in black line are the studied site in the present paper. The visible image map is also provided as shown in Fig. 5.

It can be seen from Fig. 5 that the Pearl River runs through the Haizhu district by separating into two branches and converges afterwards. For the area that surrounded by the Pearl River, the west part shows great development intensity and high building density, while the east part shows small development intensity and large green space. Above the surrounded area buildings are built intensively, while below the surrounded area buildings are built loosely. Combing Figs. 4 and 5, it can be known that there existed good relationships between LST and development intensity and land type, showing that LST was the highest for the intensively developed areas, followed by the less developed areas and roads, and LST of green and water areas were smallest. This indicated that the proposed retrieval methods were able to distinguish the surface temperature variations for different underlying urban surfaces.

The analysis of the scope marked in black line in Fig. 4 showed that the mean, maximum and minimum LST of the site were 39.8 °C, 47.9 °C and 34.2 °C, respectively. It can be seen from Fig. 5 that LST of the site was higher than other areas of Haizhu district. This probably because that the building density of the site is larger.

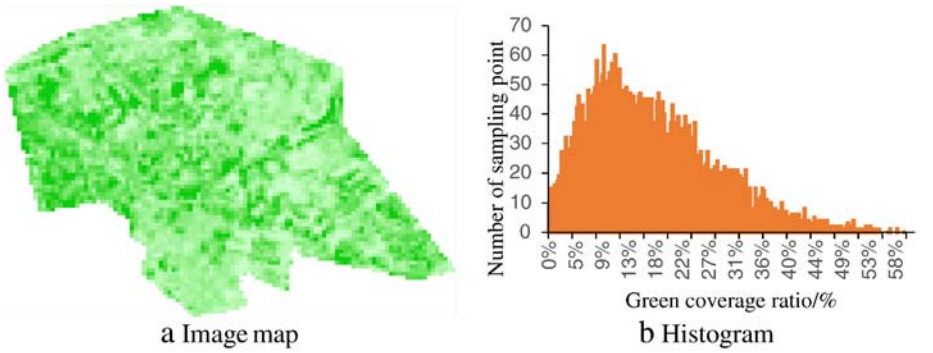

Fig. 3. Green coverage ratio of the site. (For image map, the deeper the green color, the larger the green coverage ratio is)

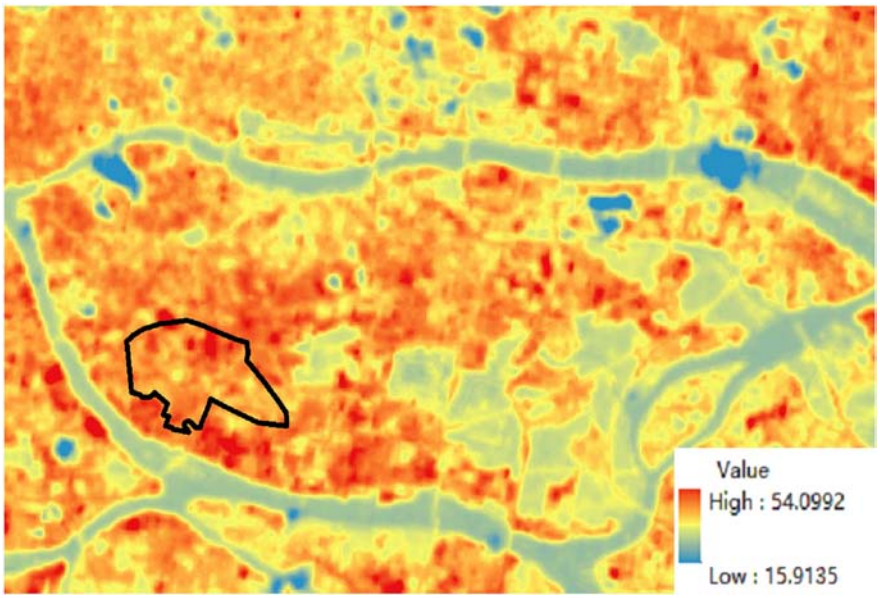

Fig. 4. LST retrieval image map of the Haizhu district in Guangzhou. (GTM 2:51 am, September 18, 2016).

The above findings were further confirmed by comparing Fig. 4 with the LCZ classification map of Haizhu district shown in Fig. 6. It can be seen that LST was the highest for the LCZ of compact buildings, followed by the LCZ of open buildings, and LST of water and vegetation were smallest. In addition, there were still some areas with low-rise buildings but high LST, and some areas with compact and middle-rise buildings but low LST, indicating that LST may be not only affected by building density and height, but also by surface pavement and greening.

Fig. 5. Visible image map of the Haizhu district in Guangzhou.

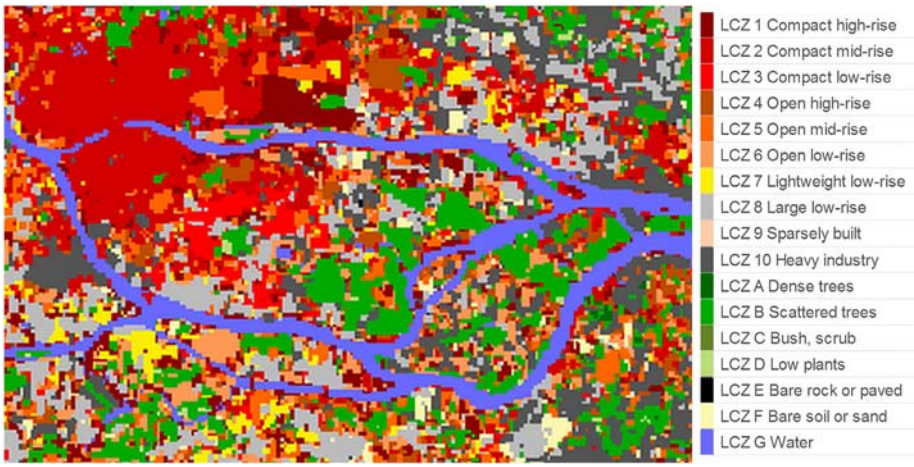
LCZ 1 Compact high-rise
LCZ 2 Compact mid-rise
LCZ 3 Compact low-rise
LCZ 4 Open high-rise
LCZ 5 Open mid-rise
LCZ 6 Open low-rise
LCZ 7 Lightweight low-rise
LCZ 8 Large low-rise
LCZ 9 Sparsely built
LCZ 10 Heavy industry
LCZ A Dense trees
LCZ B Scattered trees
LCZ C Bush, scrub
LCZ D Low plants
LCZ E Bare rock or paved
LCZ F Bare soil or sand
LCZ G Water

Fig. 6. LCZ classification map of Haizhu district in Guangzhou.
(http://geopedia.world/#T4_L107_x12622485.993643802_y2641625.479021549_s11_b17).

4.3. LST observations

Fig. 7 shows the LST observations for the patch. The higher temperatures were observed for the surfaces directly exposed to solar radiation, like the roof and part of the roads; while the lower temperatures were observed for the surfaces not exposed to direct solar radiation, like walls and vegetation. The mean surface temperatures of roof, road, walls and vegetation were 40.7 °C, 32.5 °C, 31.8 °C and 31.5 °C, respectively.

4.4. Validation of retrieval methods

As the width of Landsat image was 185 km, there might be a certain view difference that was estimated as a zenith angle of 3° between pixel of image margin and central scanning line (Qin et al., 2003). According to

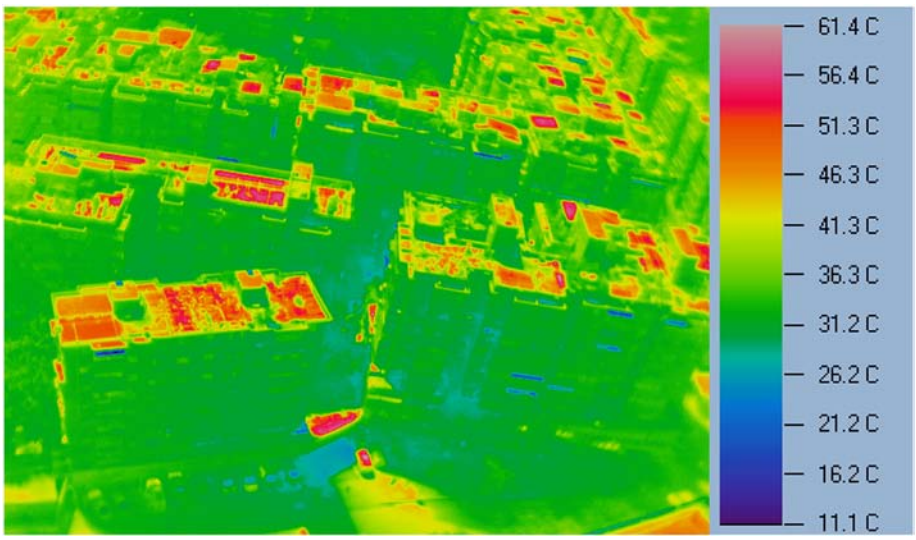

Fig. 7. Thermal infrared image of the patch.
(GTM 2:51 am, September 18, 2016).

this, the surfaces that could be observed directly from a vertical angle, including the roofs, roads, and vegetation, were considered and their average temperature was obtained as 36.8 °C based on the field observations.

The comparison between the retrieval results and the measured results reported a 3 °C difference between them. The previous studies indicated that average error of the mono-window algorithm was within 1.1 °C. Considering the accuracy of thermal Infrared camera was ±2 °C, we believed that the present study validated the results of previous studies, that is, the error of the mono-window algorithm for urban LST retrieval was about 1.0 °C. The above findings indicate that the retrieval methods based on the mono-window algorithm and the estimation methods for ground emissivity and atmospheric transmittance are applicable for urban LST retrieval in Guangzhou and other cities in the hot-humid region. Hereinafter, the cooling effects of water and vegetation on the urban LST were analyzed by using the validated retrieval methods.

4.5. Water cooling effect

The image maps of water and vegetation in Guangzhou were extracted by the NDVI threshold method as shown in Fig. 8. The NDVI values were from −1 to −0.5 for water, and 0.2– 0.8 for vegetation.

Twelve rivers in Guangzhou with various areas, lengths and widths were selected as samples to be studied. Taking water area as center, the buffer zones were built every 50 m outward (totally 10 buffer zones and 500 m away from the center), and the temperature drop, namely the mean LST of the urban land in a 500 m range outside the buffer zone minus the mean LST of the buffer zone was obtained by using ARCGIS. The change of temperature drop with buffer distance for water is shown in Fig. 9.

It can be seen that when the buffer distance became greater, the temperature drop decreased rapidly initially, and then tended to be stable with a threshold of 250 m, that is to say, the cooling effect of water on its surrounding urban lands was significant within a distance of 250 m.

Taking the LST difference between water and its cooling urban surface (300 m range) as the index of water cooling effect, the relationship between water cooling effect and water area, length and width were analyzed as shown in Fig. 10. The water cooling effect was correlated with the water area and width positively, with the correlation coefficients of 0.865 and 0.879, respectively, while independent of the water shape.

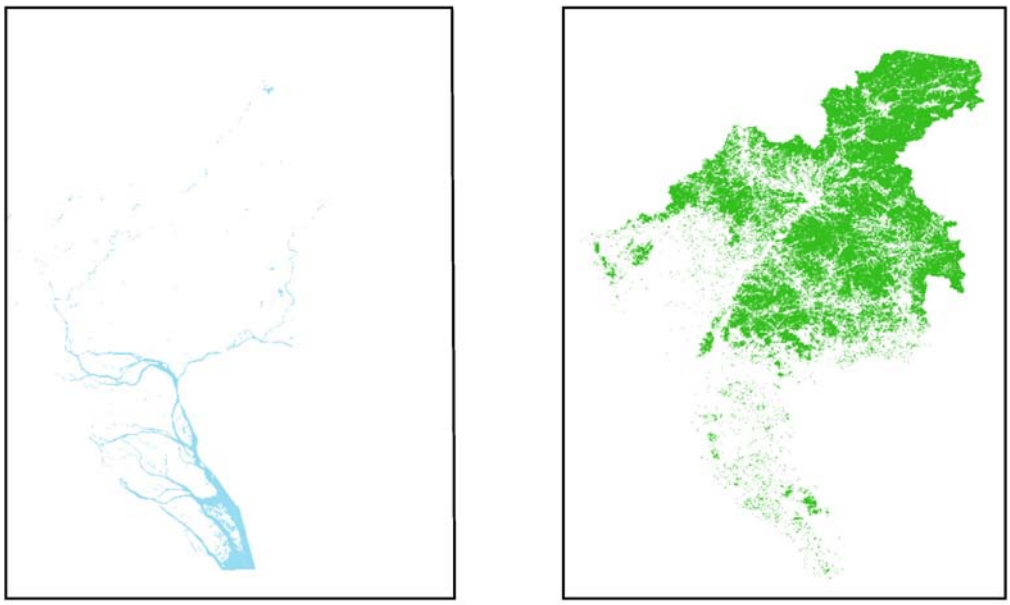

Fig. 8. Extracted image maps of water and vegetation in Guangzhou. a Water. b Vegetation.

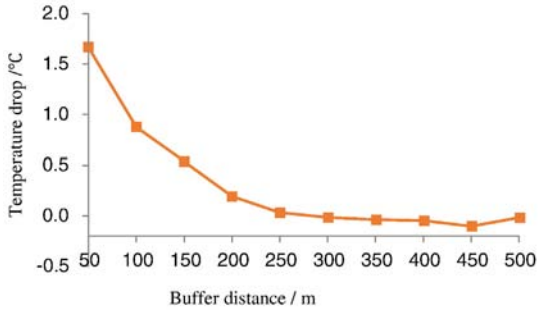

Fig. 9. Change of temperature drop with buffer distance for water.

4.6. Vegetation cooling effect

Thirteen pieces of forestry in Guangzhou with different area, shape, and canopy density were selected as samples to be studied. The definition of temperature drop and the analysis method kept the same with those of water. The results are shown in Fig. 11.

It can be seen that when the buffer distance became greater, the temperature drop decreased rapidly initially, and then tended to be stable with a threshold of 350 m. Further analysis on the relationships between

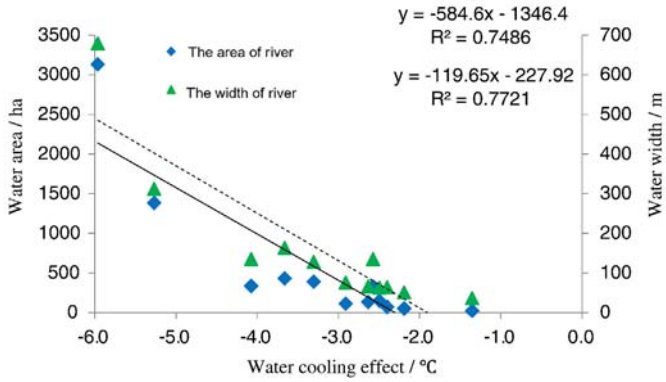

Fig. 10. Relationships between water cooling effect and water area and width.

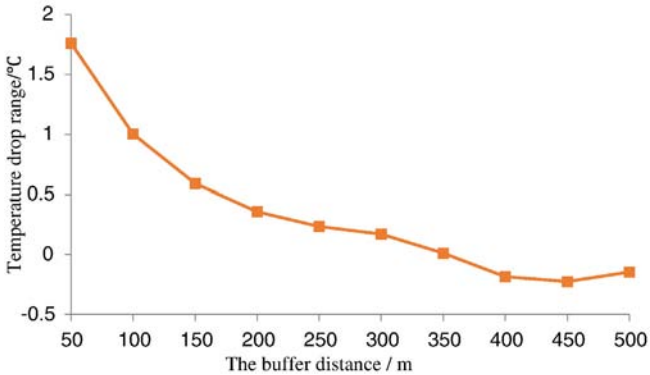

Fig. 11. Change of temperature drop with buffer distance for vegetation.

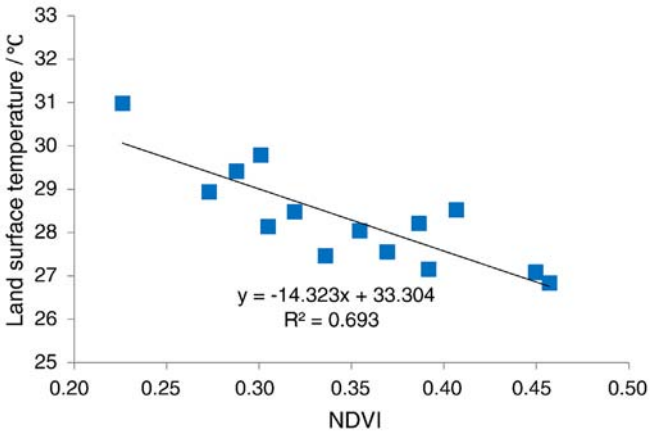

Fig. 12. Relationship between vegetation LST and NDVI.

vegetation LST and vegetation area, canopy density (represented by NDVI) and shape revealed that vegetation LST correlated with its canopy density negatively, with a correlation coefficient of −0.832 (Fig. 12), while no correlations between the vegetation LST and area or shape were found.

5. Conclusion

In this paper, the satellite-based remote sensing retrieval methods for urban LST was established based on the mono-window algorithm and the estimation methods of ground emissivity and atmospheric transmittance. Through retrieving LST of Haizhu district in Guangzhou in a sunny summer day, it was found that the retrieval methods were able to distinguish the surface temperature variations for different underlying urban surfaces. By comparison with the field observations, it was found that the error of the retrieval methods was about 1.0 °C and the methods were applicable for urban LST retrieval in the cities in the hot-humid region. The satellite-based remote sensing retrieval methods proposed and validated in the present study provide a new and reliable technique for observing and evaluating urban LST in the hot-humid region.

By applying the retrieval methods, it was shown that the cooling effects of water and vegetation on surrounding urban lands were effective within distances of 250 m and 350 m, respectively. The water cooling effect correlated with its area and width positively, and the vegetation LST correlated with its canopy density negatively. The applications of the retrieval methods on cooling effects of water and vegetation provide useful guidance for planning and design of urban climate.

Acknowledgment

The project was supported by National Natural Science Foundation of China (Project No. 51578243 and No. 51408137).

References

Bai, J., Liu, S., Hu, G., 2008. Inversion and verification of land surface temperature with remote sensing TM/ETM+ data. Transactions of the CSAE 24 (9):148–154. http://dx.doi.org/10.3321/j.issn:1002-6819.2008.09.030 (In Chinese).

Chan, A., 2011. Developing a modified typical meteorological year weather file for Hong Kong taking into account the urban heat island effect. Build. Environ. 46 (46):2434–2441. http://dx.doi.org/10.1016/j.buildenv.2011.04.038.

Chen, Y.H., Zhou, J., Gong, A.D., et al., 2014. Thermal Remote Sensing of Urban Space—Simulation of Spatial Form and Thermal Anisotropy. Science Press, Beijing, pp. 30–35 (In Chinese). ISBN: 978-7-03-039751-5.

Deng, S., 2010. ENVI Remote Sensing Image Processing Method. 305. Science Press, Beijing, China (In Chinese) ISBN:978-7-04-041066-2.

Gluch, R.Q., Saaroni, D.A., Luvall, J.C., 2006. A multi-scale approach to urban thermal analysis. Remote sensing of environment. Remote Sens. Environ. 104 (2):123–132. http://dx.doi.org/10.1016/j.rse.2006.01.025.

Gu, X., Meng, W., Yu, F., et al., 2011. Estimation of atmospheric transmittance in thermal infrared in Guiyang Band from Landsat on MODTRAN4. Chin. J. Agrometeorol. 32 (add 1), 148–152 (In Chinese).

He, H., Xu, H., 2012. Impact on thermal environment by district planning based on remote sensing technology. Plan. Stud. 36 (11), 33–38 (In Chinese).
Jimenez-Munoz, J.C., Sobrino, J.A., 2003. A generalized single-channel method for retrieving land surface temperature from remote sensing data. J. Geophys. Res. 108 (D22):4688. http://dx.doi.org/10.1029/2003JD003480.
Kaufman, Y.J., Gao, B.C., 1992. Remote sensing of water vapor in the near IR from EOS/MODIS. IEEE T Geosci Remote 30 (5):871–884. http://dx.doi.org/10.1109/36.175321.
Li, M.M., Wu, B.F., Yan, C.Z., et al., 2004. The remote sensing evaluation of green coverage ratio in upstream of Miyun reservoir. Resource Science 26 (4), 153–158 (In Chinese).
Mao, K., Qin, Z., 2004. Retrieval of water content of atmosphere in Bohai region by MODIS image. Remote Sensing Information 4:47–49. http://dx.doi.org/10.3969/j.issn.1000-3177.2004.04.014 (In Chinese).
Meng, X., Lu, S., Zhang, Y., et al., 2005. Retrieving of land surface temperature over Jinta area using LANDSAT 5 TM data. Plateau Meteorology 24 (5):721–726. http://dx.doi.org/10.3321/j.issn:1007-7588.2004.04.022 (In Chinese).
Nichol, J.E., 1996. High-resolution surface temperature patterns related to urban morphology in a tropical city: a satellite-based study. J. Appl. Meteorol. 35 (1):135–152. http://dx.doi.org/10.1175/1520-0450(1996)035<0135:HRSTPR>2.0.CO;2.
Qin, Z.H., Karnieli, A., 1999. Progress in the remote sensing of land surface temperature and ground emissivity using NOAA-AVHRR data. Int. J. Remote Sens. 20:2367–2393. http://dx.doi.org/10.1080/014311699212074.
Qin, Z.H., Karnieli, A., Berliner, P., 2001. A mono-window algorithm for retrieving land surface temperature from Landsat TM data and its application to the Israel-Egypt border region. Int. J. Remote Sens. 22:3719–3746. http://dx.doi.org/10.1080/01431160010006971.
Qin, Z.H., Li, W., Zhang, M., et al., 2003. Estimation of the essential atmospheric parameters of a mono-window algorithm for land surface temperature retrieval from Landsat TM6. Remote Sensing for Land & Resources 2 (56):37–43. http://dx.doi.org/10.3969/j.issn.1001-070X.2003.02.010 (In Chinese).
Qin, Z.H., Li, W., Xu, B., et al., 2004. The estimation of land surface emissivity for LANDSAT TM6. Remote Sensing for Land & Resources 3 (61):28–36. http://dx.doi.org/10.3969/j.issn.1001-070X.2004.03.007 (In Chinese).
Roth, M., Oke, T.R., Emery, W.J., 1989. Satellite-derived urban heat islands from three coastal cities and the utilization of such data in urban climatology. Int. J. Remote Sens. 10:1699–1720. http://dx.doi.org/10.1080/01431168908904002.
Saaroni, H., Ben-Dor, E., Bitan, A., et al., 2000. Spatial distribution and microscale characteristics of the urban heat island in Tel-Aviv, Israel. Landsc. Urban Plan. 48:1–18. http://dx.doi.org/10.1016/S0169-2046(99)00075-4.
Valor, E., Caselles, V., 1996. Mapping land surface emissivity from NDVI: application to European, African, and south American areas. Remote Sens. Environ. 57 (3):167–184. http://dx.doi.org/10.1016/0034-4257(96)00039-9.
Voogt, J.A., Oke, T.R., 1997. Complete urban surface temperatures. J. Appl. Meteorol. 36 (9):1117–1132. http://dx.doi.org/10.1175/1520-0450(1997)036<1117:CUST>2.0.CO;2.
Voogt, J.A., Oke, T.R., 1998. Effects of urban surface geometry on remotely sensed surface temperature. Int. J. Remote Sens. 19 (5): 895–920. http://dx.doi.org/10.1080/014311698215784.
Wang, W.W., Zhang, Y.Y., 2010. Quantitative analysis of controllable factors affecting thermal environment in city residential area. J. Zheijang Univ. 44 (12):2348–2353. http://dx.doi.org/10.3785/j.issn.1008-973X.2010.12.019.
Wu, W., Xiao, Y., Li, Q., et al., 2013. Temperature-mortality relationship in four subtropical Chinese cities: a time-series study using a distributed lag non-linear model. Sci. Total Environ. 449:355–362. http://dx.doi.org/10.1016/j.scitotenv.2013.01.090.
Ye, Z.W., 2009. The Relation between Neighborhood with Dense High-rises and Thermal Landscape Using Remote Sensing. Capital Normal University (In Chinese).